Fluorescence-Enhanced Photodynamic Assessments for Human Breast Cancer Cell Characterizations

Mahsa Ghezelbash *, Batool Sajad *, Shadi Hojatizadeh

Posted Date: 19 June 2024

doi: 10.20944/preprints202406.1312.v1

Keywords: fluorescence; breast cancer; detection; auto-fluorescence; key fluorophores; 5-ALA

Article

Fluorescence-Enhanced Photodynamic Assessments for Human Breast Cancer Cell Characterizations

Mahsa Ghezelbash [1,*,‡], Batool Sajad [1,*,‡] and Shadi Hojatizadeh [2]

[1] Alzahra University, Department of Atomic and Molecular Physics, Tehran, Iran; m.ghezelbash@alzahra.ac.ir; bsajad@alzahra.ac.ir
[2] Alzahra University, Faculty of Biological Sciences, Department of Biotechnology, Tehran, Iran
* Correspondence: m.ghezelbash@alzahra.ac.ir (M.G.); bsajad@alzahra.ac.ir (B.S.)
‡ These authors contributed equally to this work.

Abstract: Even with 100% certainty of a complete cure for breast cancer (BC), there is still a long way to go toward more efficient treatment. This requires sensitive and timely detection and accurate pre/post-clinical characterizations. Despite the availability of advanced diagnostic tools, many cancer patients lack access to efficient diagnostics that are both highly reliable and affordable. The fluorescence-based optical technique aims to make another significant leap forward in improving patient safety. It offers a convenient operation that reduces healthcare costs compared to visual examination tools (VETs). The primary and metastatic stages of BC consider different cancerous cell lines (MDAs), meaning the highest number of cells in this research (up to 300,000) represents the metastatic stages of BC, and 50,000 represents the primary level of BC developments have been studied based on fluorescence-enhanced photodynamic characterizations. The ability to characterize the fluorescence caused by MDA with 50,000 cells compared to the dominant radiation of MDA with 300,000 cells is emphatic proof of the high potential of fluorescence technique in timely BC detections, specifically before it spreads to the axillary lymph nodes. The specific cell numbers of 50,000 and 300,000 were chosen arbitrarily based on the cultivation of common biological limitations. Comparing the outcomes between 50,000 and 300,000 cells allows for evaluating the fluorescence technique's diagnostic capability across various stages of breast cancer. This assessment provides valuable insights into the effectiveness of the fluorescence-based characterizing approach in detecting cancerous cells at different stages of the disease. Here, we have assessed fluorescence's spectral shift and intensity difference as a diagnostic approach to distinguish between cancerous and normal breast cells. This study also presents a two-way structure of the 5-aminolevulinic acid (5-ALA) prodrug and Fluorescein Sodium (FS) effect in BC cell characterization from the perspective of photodynamical procedures and the detection side. 5-ALA induces an accumulation of protoporphyrin IX (PpIX) photosensitizer through a biosynthetic pathway, leading to red radiation of fluorescence measurements depending on different factors, such as temperature, incubation time, added glucose of the culturing medium, as well as photosynthesis processes. The presence and progression of breast cancer can be indicated by elevated levels of Reactive Oxygen Species (ROS), which are associated with the production of PpIX in cells following the administration of 5-ALA. Also, nicotinamide adenine dinucleotide (NADH) and flavin adenine dinucleotide (FAD) fluorophores are recognized as the main factors for fluorescence emissions at around 420-580 nm emission intervals. Considering the MDA's high metastatic potential, the impact of 5-ALA on MDA's cellular morphology and viability has been investigated. The molecular fluorophores are the primary probes to MDA's cellular photodynamic considerations, allowing this widespread pre/post-clinical approach. The fluorescence signal reduction due to decreased cell viability and increased MDA's cellular death rate after 24 hours of the 5-ALA-induced staining corresponds to the changes in lipid metabolism enzymes of MDAs cultured at different doses, which could be known as a cell death inducer function. Furthermore, statistical concerns have been studied using PCA multivariate component analysis to differentiate MDA cell lines administrated by 5-ALA.

Keywords: fluorescence; breast cancer; detection; auto-fluorescence; key fluorophores; 5-ALA

 doi:10.20944/preprints202406.1312.v1

1. Introduction

Breast cancer, with an increased incidence of 12%, estimated new cases of around 2 million, and 20-70% positive margins, is the most frequently diagnosed malignant in women worldwide [1–3].

The treatments proposed are continually improving, reducing the mortality rate [3–5]. However, they are still causing many early and late side effects due to the weakness of diagnostic techniques, especially in the early stages, leading to the pre/post-cancer period as a chronic condition. Consequently, moving toward well-being leads to proposing fluorescence-based structures for breast cancer cellular metabolism characterizations to consider the efficiency of treatments [6–8].

Despite expensive and complicated VETs such as X-ray mammography [9,10], MRI [11–13], and PET/CT [14,15], their inadequate accuracy in tumor residuals detection or considering cellular metabolism variations, especially in the early stages, are challenges facing this complication today [16,17]. VETs suffer from several constraints, such as large hardware, high operation costs, radio hazard risk, and disruption of the surgical workflow [18]. Various optical techniques, including optical coherence tomography (OCT) [19,20], Raman spectroscopy [21], and fluorescence lifetime imaging microscopy (FLIM) [22,23]. Hyperspectral imaging [24]have been investigated for their potential in breast cancer-characterizing cancerous breast cells, offering non-invasive approaches to obtain high-resolution images, analyze the molecular composition, study fluorescence decay rates, and detect spectral differences in tissue and cellular samples.

Fluorescence-based techniques by developing early detections could lead to a fully cured breast cancer disease because of their high sensitivity to alterations in cells' function, morphology, and microenvironment ([25]). While a low resolution still hinders the application, this procedure exhibits an ideal probe targeting the breast tumor cells based on fluorescence high quantum yield. High sensitivity with reliable and fast measurements made that a qualified method, especially for middle/low-income communities.

This study hypothesizes that fluorescence-based approaches concerning photodynamic assessments hold significant potential for accurate discrimination and characterization of cancerous and noncancerous breast cells. By utilizing 5-aminolevulinic acid (5-ALA) as a probe, this approach can effectively characterize biomarkers metabolic changes and provide valuable insights into functional and morphological alterations associated with breast cancer progression. It has been proposed to aid the characterization of various malignancies by studying pathological changes [26]. Thus, fluorescence could yield information about breast cancer's physiological states from reliable key fluorophores (KF). Among those KFs, tryptophan, collagen, elastin, reduced nicotinamide adenine dinucleotide (NADH), and flavin adenine dinucleotide (FAD) are the primary native KFs relating to BC cellular metabolic and functional processes [26–28].

Fluorescence-enhanced photodynamic assessments aimed to demonstrate the technique's potential in distinguishing between cancerous and noncancerous cells based on spectral shifts, fluorescence intensity differences, and metabolic changes, which also investigated the impact of the 5-ALA prodrug on cancer cell characterization, photodynamic processes, viability, and morphology offer valuable information about the physiological states of breast cancer. This update aims to provide a comprehensive report on the efficacy of fluorescence-enhanced photodynamic examinations as a primer for oncology in studying breast cancer cells. With a high level of trustworthiness, the update delves into the conceptual and technical foundations of the fluorescence approach. It summarises the practical and technical aspects of using the fluorescence-enhanced technique and the results obtained. Furthermore, it reviews the pathophysiological mechanisms involved and outlines the limitations to consider when applying this approach to breast cancer research.

The 5-ALA prodrug affects MDA viability, leading to a high rate of cellular death based on the applied doses of the prodrug due to its influence on intracellular transports [29]. The Reactive Oxygen Species (ROS) are produced in all cells because of normal metabolic processes, and only when their levels are significantly increased or decreased might disease be indicated. ROS could indeed be involved in cancer progression and can be used as a monitoring indicator that could cause

 doi:10.20944/preprints202406.1312.v1

genetic instability due to DNA damage or mutation load [30,31]. To detect even partial amounts of cultured MDA cells up to 50,000 indicates the high accuracy of the fluorescence-based approach, especially in early BC investigations. The apparent difference in the intensity of irradiated fluorescence for the highest amounts of breast cancer cell line (MDA) of 300,000 and other cell values spectral discrimination also proves the high sensitivity of the fluorescence technique in the study of BC. The key fluorophore molecules (likely NADH and FAD) explore cellular metabolism changes [8,32] that arise from HFF transformations to BC cells (MDAs), causing discrimination between MDAs and HFFs. MDA's different number of cells (50,000-300,000) varies fluorescence emission according to their metastatic potential, showing four times stronger emission at around 500-510 nm than HFFs. The endogenous fluorophores or auto-fluorescent molecules in the cells or the surrounding environment were observed in all 5-ALA-induced MDA cells, such as Flavin, porphyrins, and lipofuscins [33,34]. Correspondingly, 5-ALA-administered MDAs significantly reduced cell viability and highly affected cell lines' morphology according to different cell numbers of 50,000-300,000 due to their different lipid contents [29].

2. Materials and Methods

2.1. Cell Lines

For fluorescence measurements, MDA-MB-231, human foreskin fibroblast cells (HFF-2) as "control" have been cultured with six different numbers of cells of 50,000, 75,000, 100,000, 150,000, 200,000, and 300,000. Human MDA-MB-231 breast cancer and HFF-2 cell lines were purchased from the Stem Cell Research Center, STRC (Tehran, Iran) [35]. All cell lines were cultured in Dulbecco's Modified Eagle Eagle's Medium (DMEM) supplemented with 10 percent fetal bovine serum (Gibco serum albumin) and 1 percent antibiotics seeded in two 6-well cell culture plates of DMEM and incubated for 24 h (%5 CO2, 37°C, and 95% humidity). After incubation, the medium was removed and replaced with a fresh FBS. At the second level of the experiments, 5-aminolevulinic acid hydrochloride (5-ALA) was dissolved in sterile distilled water. 5-ALA administrated MDAs with six different cell amounts were prepared at a concentration of 100 μM in DMEM medium with FBS for 24h at 37 °C in a standard 6-well cell plate was then removed from the wells by trypsin, dissolved at a 1.5 ml PBS. Based on previous research and experimental considerations, the study set a 24-hour incubation time for 5-ALA with cells. Extending this time was challenging due to the large volume of the growth medium of about 3 ml and the difficulties in keeping the cells alive. After multiple tests, 24 hours was the optimal and longest feasible incubation period. Cell culturing, incubation, and fluorescence measurements also presented difficulties, making it more efficient to cultivate cells in a large volume. Hence, extending the incubation time beyond 24 hours was feasible.

Two experiments were used to acquire the spectra from cultured MDAs and HFFs separately.

Once used, a commercial HORIBA Florolog fluorometer was a proof of concept to examine the optimal excitation wavelength and consider the efficiency of the fluorescence-based feasibility. The other was the main experimental setup, designed and calibrated using proper optical components to characterize cell lines. Commercial HORIBA Florolog was an altered fluorescence spectrophotometer equipped with a xenon lamp, and the excitation was adjustable at adequate exposure times. A photomultiplier tube as a detection part allows the system to take accurate measurements. This system also assembled an adjustable cuvette holder to hold the quartz cuvette. The delay between the lamp pulse and the detector is adaptable, enabling the collection of fluorescence or phosphorescence delays. The fluorometer system was also adjustable with different slit widths from 5 to 3000 μm. The lamp illuminates samples, excitable from 210 to 800 nm.

In the second (main) experiment, a sensitive homemade spectrometer can collect light in the wavelength range of around 210 to 880 nm with a spectral resolution of 0.7 nm and an integration time of 100μs to 10s. Its configuration is highly reliable and easy to use, especially when discriminating against each sample based on spectral features. The samples were exposed at the 405 nm continuous

 doi:10.20944/preprints202406.1312.v1

wavelength of the CNI laser diode, less than 0.5 mm square, offering almost a high efficiency and lifetime compared to lamp sources. The laser can create 1 to 200 mW output power to excite samples. Despite the outstanding quality of the laser beam and the high stability, a set of filters including two bandpass filters (390nm CWL, 25mm Dia, 40nm Bandwidth, OD 6, 86-348, Edmond Optics) tilted at 5-7 degree were use to narrow wide pass-band in the excitation leg. Then, using two UV-fused silica plano-convex lenses with 50 mm focal lenses shown as optics block (O), the paralyzed passing beam led to the center of the quartz cuvette embedded at the center of the holder, shown in the schematic figure of the schema at Figure 1. UV fused silica plano-convex lenses were selected due to their unique features on fluorescence applications. Exposing them to the beam pass will not lead to excess fluorescent radiation from the lenses themselves and reduce the sensitivity of the measurements. To capture the graphical morphology from a CMOS (E3ISPM, LaboQuip Digital Camera) camera coupled with an achromatic objective lens (VIS-20X-95-NA0, 300-800 nm) was used as shown in Figure 1 schema. In the end, fluorescence emission was collected and guided through the spectrometer's entrance using two 409 nm dichroic long-pass filters (Edmond Optics) tilted at 5 to 7 degrees, along with two 50 mm UVFused silica plano-convex lenses shown as collection optics block (CO) in Figure 1. The setup was also covered with a non-fluorescent box to prevent annoying environmental noise.

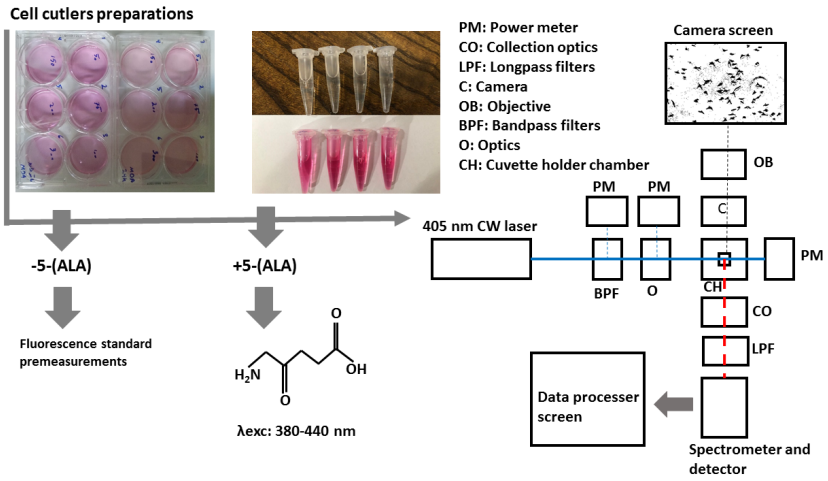

Figure 1. Schematic setup for cell lines fluorescence characterizations.

2.2. *Statistical Analysis*

Statistical analyses and graphs were performed using MATLAB, Excel, OriginPro, and SPSS software. The software SPSS has been used to plot and interpret multiple comparisons. All experiments were prepared and analyzed numerous times, and the obtained data were presented as the mean ± SD.

3. Results and Discussion

3.1. *MDA Pre-Investigations*

The birth of the research, mainly for timely BC detections, required collecting a detailed database using the studies carried out in this field until now. It then conducted preliminary practical examinations using any equipment on the BC cellular changes and investigated using Florolog as a necessary part to evaluate fundamental ideas. Considering the initial point of this research as the zero stage, this is regarded as a (-1) level, evaluating the initial feasibility of the investigation and the proof of concept. MDAs prepared with six different numbers of cells of 50,000, 75,000, 100,000, 15,000, 200,000, and 300,000 have been carried out to qualitatively examine their collected fluorescence changes and the sensitivity of measurements. As can be seen in Figure 2, MDAs and HFFs at six different numbers of cells of 50,000-300,000 were subjected to collecting fluorescence emission spectra (excitation/emissions at 405 nm/420-600 nm) using a standard spectrofluorometer (Horiba Scientific, Edison, NJ, USA)

 doi:10.20944/preprints202406.1312.v1

equipped with a quartz cuvette holder. The fluorescence spectra were recorded from 1 ml of each cell line. The obtained data were corrected from the blank quartz cuvette and ambient. For 405 nm excitation, a predominant native fluorophore at around 420-480 nm and 480-530 nm regarded NADH and FAD, respectively, with an almost high quantum efficiency depending on the local environment and protein structures, shows the most significant spectral discrepancy, which could count as convenient to maximize cancer discrimination [8,28,32].

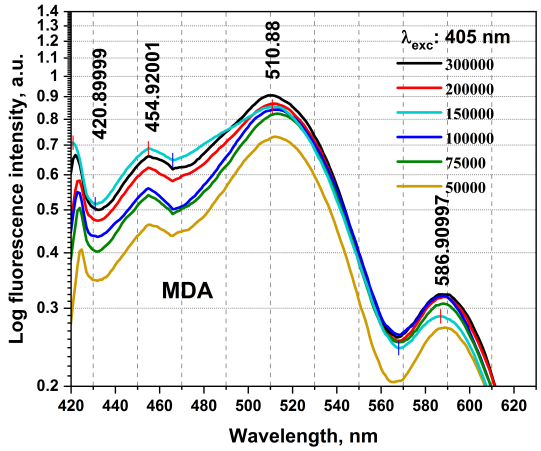

Figure 2. The fluorescence spectra registered from the excised MDA specimen were obtained from different cellular numbers of 50,000, 75,000, 100,000, 150,000, 200,000, and 300,000. Each measurement was tested in three independent experiments (n=3)

To highlight the spectral differences among MDAs with varying cell counts (from 50,000 to 300,000), we compared the obtained fluorescence excited at 405 nm at the prominent spectral characterized peaks of 420, 454, 510, and 556 nm (Figure 3 and Table 1), highlighting the spectral differences among MDAs with different cells from 50,000 to 300,000. The fluorescence-enhanced photodynamic assessments provide accurate discrimination between MDAs and HFFs using direct exposure to FS as a natural photosensitizer, which has been used at the forefront of cell metabolism investigations [36,37]. The HFF-2 cell line represents fibroblast cells with elongated and spindle-shaped morphology, which are the most abundant among connective tissue cells. The primary function of fibroblasts is the structural cohesion of connective tissue, which counts as a "control." Due to some features, such as being accessible to culturing, longer life, and the high structural similarity of these cells to the human breast cells, they were very efficient, especially in comparing the cellular viability or death of these cells with MDA cells applying 5-ALA prodrug. Likewise, 5-ALA-induced PpLX is a potent fluorescent agent [38,39] and a photosensitizer favored in malignant and premalignant cells, making it an excellently targeted probe in photodynamic considerations [40–42]. Reactive Oxygen Species (ROS) are by-products of aerobic metabolism and can act as signaling molecules to participate in multiple regulation of biological and physiological processes [43]. Hydrogen Peroxide (H_2O_2), superoxide anion (O_2^-), hypochlorous acid (HOCl), singlet oxygen ($^1O_2$), and hydroxyl radical (·OH), and act as second messengers in cell signaling, and are essential for various biological processes in normal and cancer cells [44]. The occurrence, growth, metastasis of tumors, and even the apoptosis, necrosis, and autophagy of tumor cells are all closely related to ROS [43]. 5-aminolevulinic acid (5-ALA) is a non-fluorescent prodrug that can be metabolized into fluorescent protoporphyrin IX (PpIX) in cells often used in photodynamic therapy (PDT) for cancer treatment. In this process, 5-ALA is administered to the patient, accumulating in the cancer cells. When exposed to a specific wavelength of light, the PpIX is activated and produces ROS, which can cause cell death.

 doi:10.20944/preprints202406.1312.v1

Table 1. Wavelength specifications.

Index	Beginning x (nm)	Ending x (nm)	FWHM (nm)	Central wavelength (nm)	Height
420.9 nm	409.8	30.9	15.4	420.9	0.7
454.9 nm	430.9	465.8	32.9	454.9	0.6
510.8 nm	465.9	567.9	80.6	510.9	0.8
586.9 nm	567.9	643.9	48.4	556.9	0.2

MDAs show an increased NADH fluorophor significantly at around 454 nm and FAD at 510 nm emissions compared to each other could be related to the different other fluorophores most likely [8,45]. The minimum number of cells is 50,000 (early BC), which is targeted to evaluate the detection ability of the fluorescence platform preclinical assays. It shows the comparison of the lowest fluorescence intensity compared to 300,000 (advanced BC) on different wavelengths of 420, 545, 510, and 556 nm, admitting that any MDA cellular changes (metabolism) [37,46] could happen fluorescence variations, clarify fluorescence's ability to detect, especially in early BC.

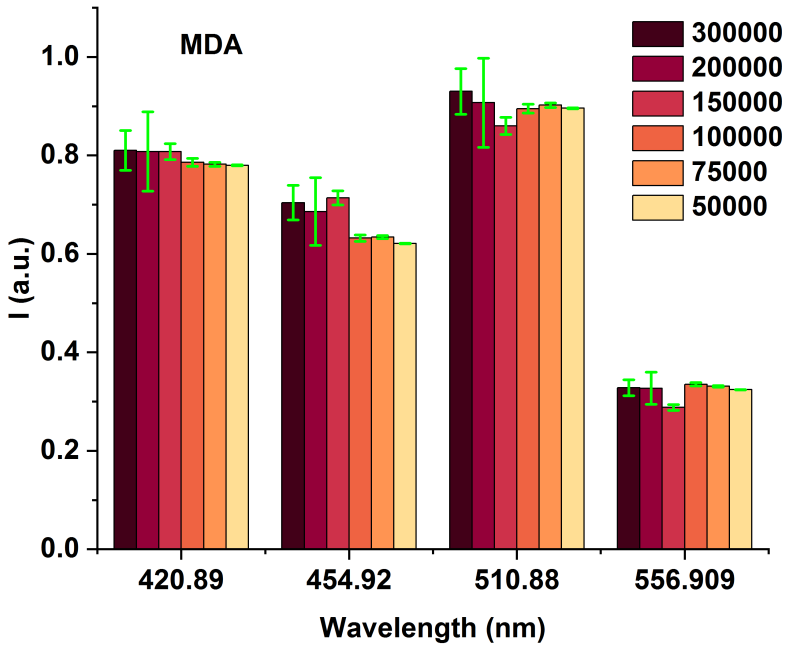

Figure 3. Bar graphs of different MDA cell numbers of 300,000, 200,000, 150,000, 100,000, 75,000, and 50,000 fluorescence intensity correspond to 420, 454, 510, and 554 nm emission wavelengths under 405 nm excitation.

3.2. MDAs and HFFs Experimentation

It could also be considered a comparison of the fluorescence variation profiles regarding MDAs and HFFs through increasing the numbers of cells in the emissions areas of 475-545 nm under the 405 nm excitation wavelength given (Figure 4). Exposing samples at 405 nm excitation using the designed fluorescence platform (Figure 1) ignited Fluorescence-enhanced photodynamic assessments. It can be seen that MDAs exhibit fluorescence emission almost four times more substantial than that of HFFs at the same wavelength region belonging to 300,000 cells, as Figure 4 a and b. In contrast, HFFs exhibit equal or minor intrinsic fluorescence signal variation rates (c and d).

 doi:10.20944/preprints202406.1312.v1

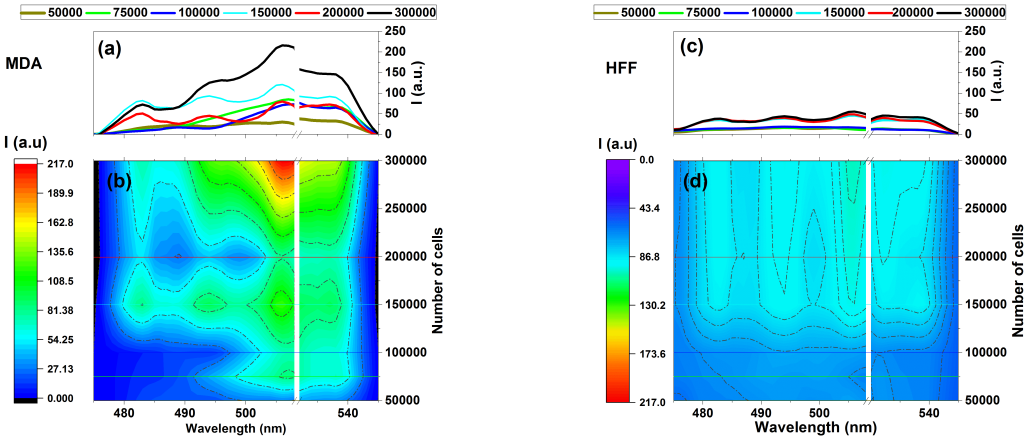

Figure 4. Fluorescence intensity vs. the number of cells for (a and b) MDAs and (c and d) HFFs at an excitation/emission of 405nm/ 454-545 nm correspond to the fluorescence of NADH at different numbers of cells of 50,000, 75,000, 100,000, 150,000, and 200,000. Each measurement was tested via three independent experiments (n=3)

Note that rapid measurements were recommended in this research since there was a higher possibility for cell destruction in case of extended measures due to being cells longer out of standard storage conditions. The time to measure a complete set of prepared cells (6 different samples each day) needed at least 20 minutes. Therefore, the obtained sets were averaged accordingly and needed at least three measurements repeated on different working days, which helped us compare the data each day with a minimum error.

However, there is a noticeable difference in intensity between the fluorescence data of MDAs and HFFs, especially around the 500 to 530 nm emission area with four distinct regions at around 480, 500, 510, and 530 nm that could be arising from essential coenzymes [7,8]. Based on existing literature, NADH and FAD could be the most blocking coenzymes emitting around 480 to 540 nm and highly depend on their cells' lipid metabolism enzyme changes, corresponding to fluorescence variation [6,47–49].

3.3. The 5-ALA Authority in the MDA's Cellular Viability and Morphology

- MDA's cellular morphology

The potential death mechanism induced by 5-ALA prodrug and its treatment effects has been investigated. 5-ALA prodrug has an essential impact on the BC cell morphology that has been evaluated (Figures 5 and 6). The phase-contrast images were captured using a camera setup consisting of a microscope (XDS-1B inverted biological lab microscope) attached with a CMOS camera (Toupcam-U3CMOS-10000KPA, 10 MPix) and a proper camera lens in which the cultured cells before/after incubation adding ALA directly from a 6-well cell plate was illuminated perpendicularly using a LED white light source. The attached microscope then collects the reflected light with a standard objective lens with a focal distance of f = 200mm. Captures of a CMOS camera monitored the cellular morphology of MDAs before and after 5-ALA administrations for about 24 hours. As shown in Figure 5a, MDAs Inherently display polyhedral morphology, causing them with low metastatic potential ([50,51]). While cell treatment 5-ALA-administered MDAs accumulates, cells appear more rounded than untreated MDAs Figure 5b.

 doi:10.20944/preprints202406.1312.v1

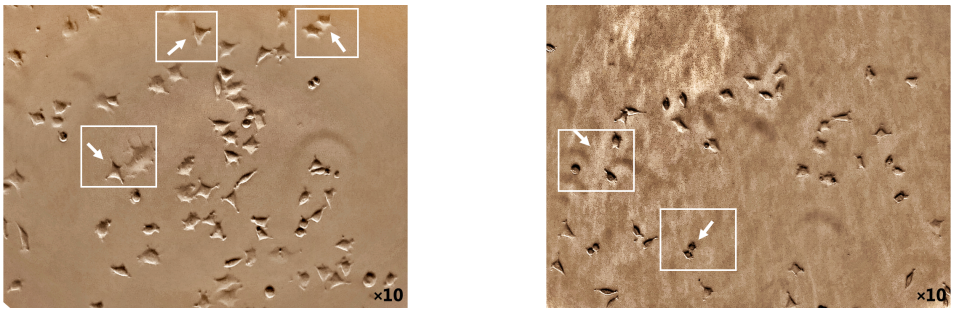

(a) (b)

Figure 5. Cellular morphology of control MDA human breast cancer cells monitoring at 50,000 number of the cell before and after 1mM of 5-ALA treatment for 48 h by phase-contrast photos.

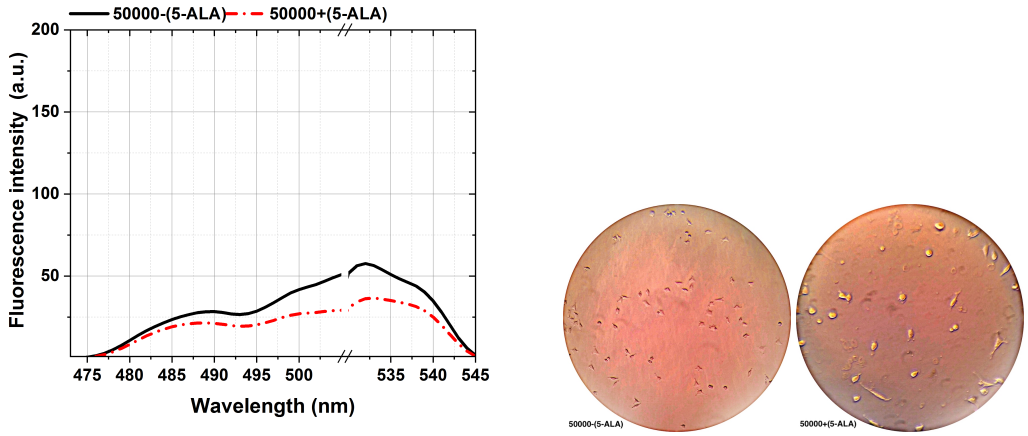

(a)

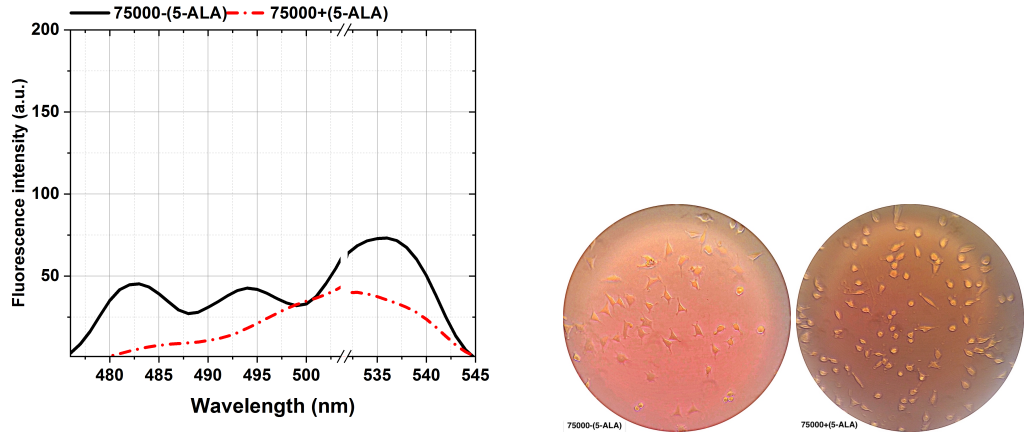

(b)

Figure 6. *Cont.*

 doi:10.20944/preprints202406.1312.v1

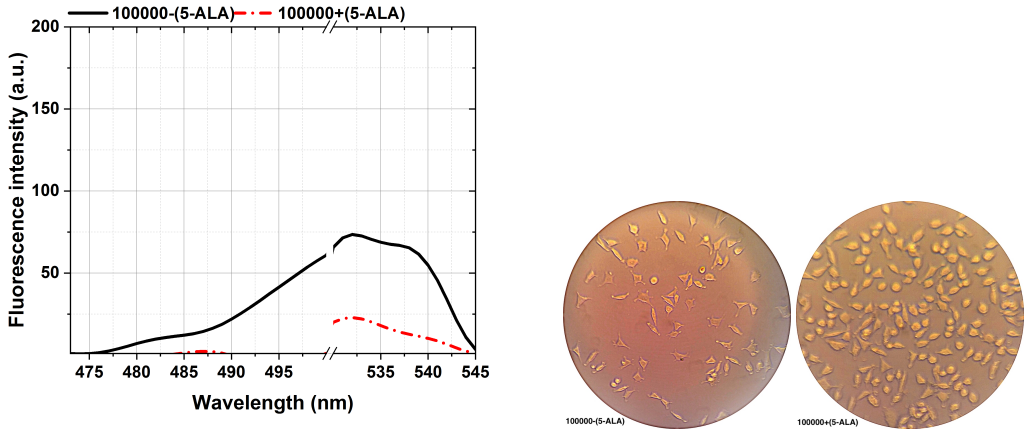

(c)

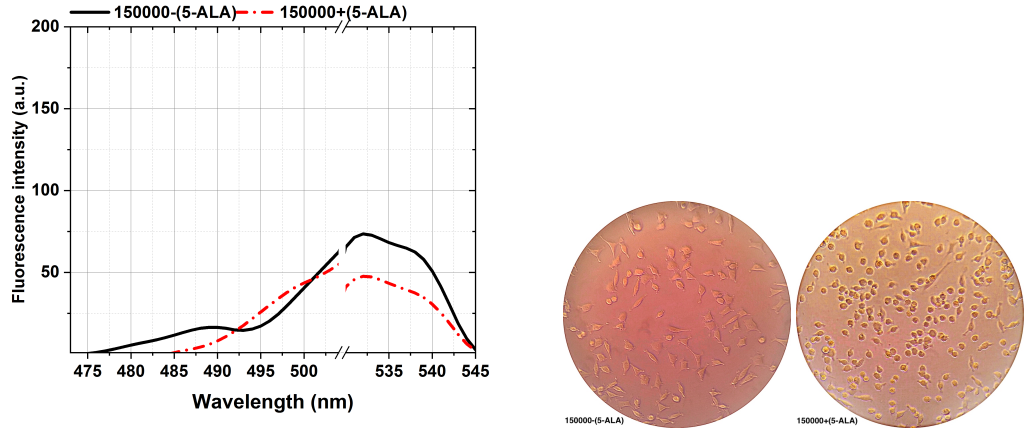

(d)

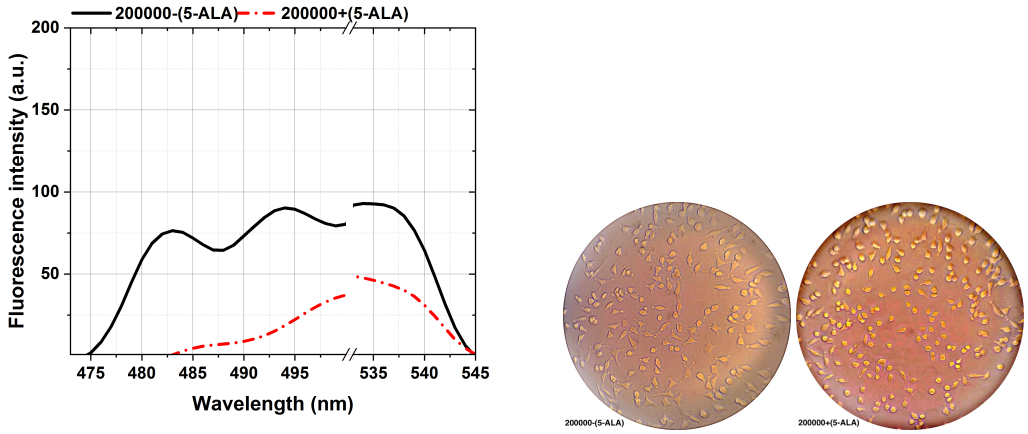

(e)

Figure 6. *Cont.*

 doi:10.20944/preprints202406.1312.v1

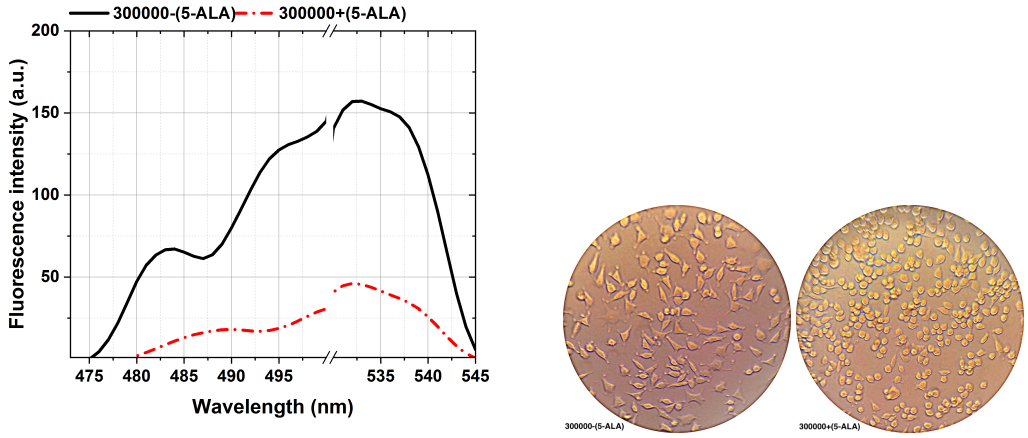

(f)

Figure 6. Comparison of the fluorescence spectra (left plots) and different MDAs cellular shapes (right photos) from different MDAs number of cells (50,000-300,000), assisted with 5-ALA and without excited at 405 nm excitation. Scale bars, 100 mm. Each measurement was tested in three independent experiments (n=3)

The ability to reveal the decreasing fluorescence signal caused by the 5-ALA-affected MDA cell lines is from the other side stepping forward through photodynamic considerations of BC characterizations. That is an efficient approach to characterizing BC, showing a clear difference between 5-ALA-assisted and not-assisted MDAs in spectral areas of around 480-540 nm, as shown in Figure 6. According to the cellular shape and fluorescence intensity of spectra, 5-ALA-assisted MDAs (a-f) show lower fluorescence intensities than untouched 5-ALAs.Our results complement that 5-ALA-assisted MDAs lead to a higher rate of cellular death and deformation rate, which decreases the fluorescence obtained [52,52,53]. This effect is because absorbing 5-ALA by BC cells and exciting at 405 nm, making 5-ALA produce oxygen radicals, leading to MDAs cellular death [7]. The fluorescence spectra of the 480-540 nm spectral areas differ slightly from the ALA-assisted MDAs, especially at the lowest number of cells from 50,000(a) than the maximum number of cells (f).

Enhancing a higher visualizing of the spectra variability, about 0.01 ml sodium fluorescein (SF) as a fluorescent dye ([37]) with a molecular weight of 376 g/mol has accumulated on each MDA with a different cell number of 50,000-300,000 through 6 different standards 1 ml micro-tube. Then, each sample was vortexed for 30 seconds, which prolonged exposure to 1ms of the activating 405 nm excitation marked obtained fluorescence assays with further implications potential.

The results demonstrate the potential of a fluorescence-based technique in distinguishing between cancerous and noncancerous breast cells based on spectral shifts, fluorescence intensity differences, and metabolic changes associated with tumor initiation and progression. Our objective was to assess the overall diagnostic capability of the fluorescence-based technique in characterizing breast cancer cells. The varying numbers of cells were utilized to investigate the impact of cell concentrations and characterization potential of 5-aminolevulinic acid (5-ALA), a prodrug used in fluorescence-enhanced photodynamic assessments By culturing breast cancer cells (MDAs) and normal human cells (HFFs) with different numbers of cells (ranging from 50,000 to 300,000), we aimed to evaluate how cell concentrations influence the uptake and subsequent fluorescence characteristics of the 5-ALA. While higher cell numbers are expected to decrease the uptake per individual cell, studying a range of cell concentrations allows us to assess the overall fluorescence signal and its detection implications. The objective was to understand the relationship between cell concentrations, 5-ALA, and the resulting fluorescence emissions. This information is crucial for determining the optimal conditions and cell concentrations for a reliable and effective fluorescence-based solution. Administering 5-ALA induces PpLX directly into cultured cells and, after incubation, accumulates PpIX photosensitizer through a biosynthetic pathway. Based on the studies, it is expected that applying 5-aminolevulinic acid

 doi:10.20944/preprints202406.1312.v1

(5-ALA) causes the production of another biomarker named protoporphyrin IX (PpIX) as a part of fluorescence emissions, measurements sensitivity to cell detections and characterizations. Accordingly, it is supposed to appear at a peak around 620 and 634 nm (a reddish fluorescence), applying 405 nm light. In comparison, the main emission interval (in this work) was around 420 to 600 nm (Figure 2) and 470-545 nm (Figure 6); hence, the fluorescence emission of PpIX is removed. It could be known to be pH-related [54,55] or link pathological status, and the gene expressions in vivo rely on a different aggregate of PpIX [56–58]. Also, other influential factors, such as temperature, incubation time, and added glucose of the culturing medium, influence the relative porphyrin concentrations, causing a faster photo-bleaching rate of the Pp spectrum [54,59,60].

3.4. Multivariate Cell Lines Analysis

Principal Component Analysis (PCA) was used to objectively differentiate between the MDAs, HFFs, and the 5-ALA-administered MDAs. Figure 7 shows the PCA of 10 different measurements discontinuously for the principal components 1 and 2 in a plane. The scattering of the data points, which are a hollow blue triangle for HFFs, open black circles for MDA-(5-ALA), and solid red circles for MDA+ (5-ALa), visualizes the possibility of differentiating between them and the reproducibility from one measurement to another. PCA was done on ten sets of cultured MDAs with a different number of cells of 50,000, 75,000, 100,000, 150,000, 200,000, and 300,000 during a similar cultural process separately. The fluorescence spectra of the MDAs and HFFs show intensity peaks at around 480 to 540 nm. Principle components one (PC1) and two (PC2) represent the data set from the fluorescence spectra excited at 405 nm. All experiments were repeated at least three times (n=3). The obtained data was presented as the mean ± standard deviation.

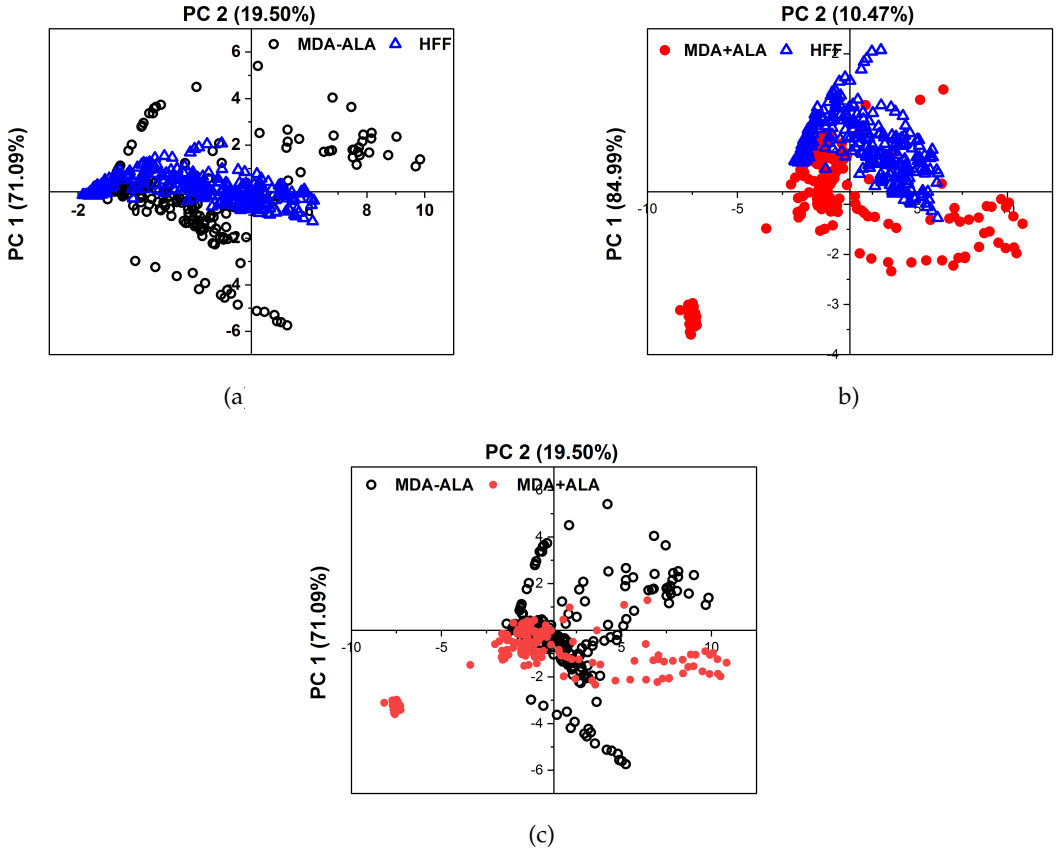

Figure 7. Comparison of the PCA results between (a) MDA (without ALA) and HFF, (b) MDA (with ALA) and HFFs, and (c) MDAs assisted with and without ALA at 405 nm excitation. Data was repeated over ten times in the calculation.

 doi:10.20944/preprints202406.1312.v1

The higher concentration of hollow blue triangle for HFFs rather than MDA-(5-ALA) indicates that the obtained fluorescence spectra of HFF are reproducible, irrespective of measurements. The clear separation of the HFF data (triangles) and from the MDAs (circles) indicates that the obtained fluorescence spectra of HFF can be separated from MDAs. It is also considered that the dispersion of the data in the case of MDA+(5-AlA) has more similarity to the HFFs (with the first principal component 84.99% of the total variance in the fluorescence spectra of Figure 7b).

While the PCA graph displays variability, which is anticipated due to the inherent biological differences in cell lines, even under similar culture conditions, this variability stems from factors such as genetic drift[61], variation in cell culturing conditions[62], genomics variations or epigenetic modifications [63,64], PCA refactors [65] and cell cycle stage disparities at the time of analysis. The number of cells can influence the intensity of the PCA graph, but it can also introduce variation if the cells are at different growth or confluence stages. In essence, the PCA graph's variation results from the multidimensional nature of the data, which may not be fully represented in other graphs. The PCA graph offers a multidimensional data perspective and is not designed to differentiate between individual groups. Instead, it provides a comprehensive view of the overall data structure and relationships. The overlapping groups in the PCA graph signify the biological similarities among the cell lines and the subtle effects of the treatment.

4. Conclusions

This research highlights the high potential of fluorescence-based approaches for accurate discrimination and characterizations between cancerous and noncancerous cells based on biological changes associated with tumor initiation and progression as the main idea of Fluorescence-enhanced photodynamic assessments. Noncancerous dermal fibroblast cells (HFFs) and cancerous cells (MDAs) with primary (50,000) up to advanced (300,000) metastatic stages of BC were growing under standard laboratory situations. In summary, using different cell numbers in the study may serve to investigate the relationship between cell concentration and fluorescence emission and provide insights into the behavior of cancerous cells at various stages of breast cancer. However, it is essential to consider the potential impact of cell concentration on the uptake of ALA and interpret the results accordingly for future work. When 5-ALA is administered, it accumulates in cancer cells and is metabolized to protoporphyrin IX (PpIX). When PpIX leads to cell death. However, the specific dose of ROS that can induce cell death can vary depending on the type of cell, the cellular environment, and other factors. It is also important to note that ROS can cause cell death but plays a vital role in normal cellular functions. The metabolic changes of the cells under the influence of the induced (bio) chemical factor, such as 5-ALA, validate its biological activity based on spectral shifts, and fluorescence intensity differences are keys to characterizing BC cells for pre/post-clinical applications.

Photo-dynamical reactions of the fluorophore probes after 5-ALA registering and fluorescein sodium (FS) administration have also been studied, principally considering the cellular viability and visualization booster. Thus, after 24 h of 5-ALA stimulation, the MDA cells manifested significant cellular viability based on their morphology changes. The efficacy of 5-ALA prodrug on the higher number of MDA cells (200,000) in treating advanced breast cancer has already been revised in the literature.

It was considered that after 5-ALA administration to MDAs, the cells are rapidly metabolized, owing to changes in the activity of enzymes and highly affecting their BC cell viability, decreasing fluorescence emission. The results also show a particular aspect of 5-ALA prodrug on MDAs, suppressing BC cells spreading to the surrounding areas, especially the axillary lymph nodes, preventing their progress, which can significantly affect cancer treatment. Comparing the microscopic images of MDA cells assisted with and without 5-ALA prodrug on the morphology of the cells could claim this approach as photodynamic procedures showing up as the other sides of the obtained results.

 doi:10.20944/preprints202406.1312.v1

Author Contributions: M. Gh. and B. S. contributed equally to this paper. Sh. H. from the biological group collected and prepared the total MDA and HFF cell lines. Sh. H. also participated in the interpretation of results and data finalization.

Funding: This research was funded by the Center of International Science and Technology Cooperation (CISTC) funding agency and Alzahra University in Tehran, Iran.

Institutional Review Board Statement: Not applicable.

Data Availability Statement: The corresponding authors' data supporting this study's findings are available upon reasonable request.

Acknowledgments: This work was supported by Alzahra University in Tehran, Iran. The authors thank Dr. Reihaneh Ramezani, AP of the Nanobiotechnology research group from the Women Research Center at Alzahra University, for her scientific and technical assistance with MDA-MB-231 and HFF cell line preparations.

Conflicts of Interest: The authors declare that they have no competing interests.

References

1. Lauwerends, L.J.; Abbasi, H.; Schut, T.C.B.; Driel, P.B.A.A.V.; Hardillo, J.A.U.; Santos, I.P.; Barroso, E.M.; Koljenović, S.; Vahrmeijer, A.L.; de Jong, R.J.B.; et al. The complementary value of intraoperative fluorescence imaging and Raman spectroscopy for cancer surgery: combining the incompatibles. *European Journal of Nuclear Medicine and Molecular Imaging* **2022**, *49*, 2364–2376. https://doi.org/10.1007/s00259-022-05705-z.
2. Morita, M.; Tanaka, H.; Kumamoto, Y.; Nakamura, A.; Harada, Y.; Ogata, T.; Sakaguchi, K.; Taguchi, T.; Takamatsu, T. Fluorescence-based discrimination of breast cancer cells by direct exposure to 5-aminolevulinic acid. *Cancer Medicine* **2019**, *8*, 5524–5533. https://doi.org/10.1002/cam4.2466.
3. Unger, J.; Hebisch, C.; Phipps, J.E.; Lagarto, J.L.; Kim, H.; Darrow, M.A.; Bold, R.J.; Marcu, L. Real-time diagnosis and visualization of tumor margins in excised breast specimens using fluorescence lifetime imaging and machine learning. *Biomedical Optics Express* **2020**, *11*, 1216. https://doi.org/10.1364/BOE.381358.
4. Zheng, Y.; Yang, H.; Wang, H.; Kang, K.; Zhang, W.; Ma, G.; Du, S. Fluorescence-guided surgery in cancer treatment: current status and future perspectives. *Annals of Translational Medicine* **2019**, *7*, S6–S6. https://doi.org/10.21037/atm.2019.01.26.
5. Ju, Y.; Dong, B.; Yu, J.; Hou, Y. Inherent multifunctional inorganic nanomaterials for imaging-guided cancer therapy. *Nano Today* **2019**, *26*, 108–122. https://doi.org/10.1016/j.nantod.2019.03.006.
6. Eiriksson, F.F.; Nøhr, M.K.; Costa, M.; Bödvarsdottir, S.K.; Ögmundsdottir, H.M.; Thorsteinsdottir, M. Lipidomic study of cell lines reveals differences between breast cancer subtypes. *PLOS ONE* **2020**, *15*, e0231289. https://doi.org/10.1371/journal.pone.0231289.
7. Melanthota, S.K.; Kistenev, Y.V.; Borisova, E.; Ivanov, D.; Zakharova, O.; Boyko, A.; Vrazhnov, D.; Gopal, D.; Chakrabarti, S.; K, S.P.; et al. Types of spectroscopy and microscopy techniques for cancer diagnosis: a review. *Lasers in Medical Science* **2022**, *37*, 3067–3084. https://doi.org/10.1007/s10103-022-03610-3.
8. Palmer, G.M.; Keely, P.J.; Breslin, T.M.; Ramanujam, N. Autofluorescence Spectroscopy of Normal and Malignant Human Breast Cell Lines. *Photochemistry and Photobiology* **2003**, *78*, 462. https://doi.org/10.1562/0031-8655(2003)078<0462:ASONAM>2.0.CO;2.
9. Chae, E.Y.; Kim, H.H.; Sabir, S.; Kim, Y.; Kim, H.; Yoon, S.; Ye, J.C.; Cho, S.; Heo, D.; Kim, K.H.; et al. Development of digital breast tomosynthesis and diffuse optical tomography fusion imaging for breast cancer detection. *Scientific Reports* **2020**, *10*, 13127. https://doi.org/10.1038/s41598-020-70103-0.
10. Moghaddam, A.A.; Sajad, B.; Nia, F.M.; Madani, S.H. Cancerous Tissue Diagnosis by LIF Spectroscopy Derived From Body-Compatible Fluorophores. *Journal of Lasers in Medical Sciences* **2021**, *12*, e10–e10. https://doi.org/10.34172/jlms.2021.10.
11. Stewart, H.L.; Birch, D.J.S. Fluorescence Guided Surgery. *Methods and Applications in Fluorescence* **2021**, *9*, 042002. https://doi.org/10.1088/2050-6120/ac1dbb.
12. Ottolino-Perry, K.; Shahid, A.; DeLuca, S.; Son, V.; Sukhram, M.; Meng, F.; Liu, Z.; Rapic, S.; Anantha, N.T.; Wang, S.C.; et al. Intraoperative fluorescence imaging with aminolevulinic acid detects grossly occult breast cancer: a phase II randomized controlled trial. *Breast Cancer Research* **2021**, *23*, 72. https://doi.org/10.1186/s13058-021-01442-7.
13. Woo, Y.; Chaurasiya, S.; O'Leary, M.; Han, E.; Fong, Y. Fluorescent imaging for cancer therapy and cancer gene therapy. *Molecular Therapy - Oncolytics* **2021**, *23*, 231–238. https://doi.org/10.1016/j.omto.2021.06.007.

 doi:10.20944/preprints202406.1312.v1

14. kyoung Shin, Y.; Eom, J.B. Optical Imaging Technology for Real-time Tumor Monitoring. *Medical Lasers* **2021**, *10*, 123–131. https://doi.org/10.25289/ML.2021.10.3.123.
15. Ugwah, J.A.; O'Sullivan, M.; O'Donnell, B.; Moore, E.J. Recent Advances in Development of New Technology in Pre and Intra Operative Breast Cancer Diagnoses. *Journal of Cancer Treatment and Diagnosis* **2021**.
16. Tummers, W.S.; Warram, J.M.; Tipirneni, K.E.; Fengler, J.; Jacobs, P.; Shankar, L.; Henderson, L.; Ballard, B.; Pfefer, T.J.; Pogue, B.W.; et al. Regulatory Aspects of Optical Methods and Exogenous Targets for Cancer Detection. *Cancer Research* **2017**, *77*, 2197–2206.
17. Yang, R.; Wang, P.; Lou, K.; Dang, Y.; Tian, H.; Li, Y.; Gao, Y.; Huang, W.; Zhang, Y.; Liu, X.; et al. Biodegradable Nanoprobe for NIR-II Fluorescence Image-Guided Surgery and Enhanced Breast Cancer Radiotherapy Efficacy. *Advanced Science* **2022**, *9*, 2104728. https://doi.org/10.1002/advs.202104728.
18. Alam, M.W.; Wahid, K.A.; Goel, R.K.; Lukong, K.E. Development of a low-cost and portable smart fluorometer for detecting breast cancer cells. *Biomedical Optics Express* **2019**, *10*, 399. https://doi.org/10.1364/BOE.10.000399.
19. Nguyen, F.T.; Zysk, A.M.; Chaney, E.J.; Kotynek, J.G.; Oliphant, U.J.; Bellafiore, F.J.; Rowland, K.M.; Johnson, P.A.; Boppart, S.A. Intraoperative Evaluation of Breast Tumor Margins with Optical Coherence Tomography. *Cancer Research* **2009**, *69*, 8790–8796. https://doi.org/10.1158/0008-5472.CAN-08-4340.
20. Yang, H.; Zhang, S.; Liu, P.; Cheng, L.; Tong, F.; Liu, H.; Wang, S.; Liu, M.; Wang, C.; Peng, Y.; et al. Use of high-resolution full-field optical coherence tomography and dynamic cell imaging for rapid intraoperative diagnosis during breast cancer surgery. *Cancer* **2020**, *126*, 3847–3856. https://doi.org/10.1002/cncr.32838.
21. Githaiga, J.I.; Angeyo, H.K.; Kaduki, K.A.; Bulimo, W.D.; Ojuka, D.K. Quantitative Raman spectroscopy of breast cancer malignancy utilizing higher-order principal components: A preliminary study. *Scientific African* **2021**, *14*, e01035. https://doi.org/10.1016/j.sciaf.2021.e01035.
22. Ouyang, Y.; Liu, Y.; Wang, Z.M.; Liu, Z.; Wu, M. FLIM as a Promising Tool for Cancer Diagnosis and Treatment Monitoring. *Nano-Micro Letters* **2021**, *13*, 133. https://doi.org/10.1007/s40820-021-00653-z.
23. Liu, L.; Yang, Q.; Zhang, M.; Wu, Z.; Xue, P. Fluorescence lifetime imaging microscopy and its applications in skin cancer diagnosis. *Journal of Innovative Optical Health Sciences* **2019**, *12*. https://doi.org/10.1142/S1793545819300040.
24. Aboughaleb, I.H.; Aref, M.H.; El-Sharkawy, Y.H. Hyperspectral imaging for diagnosis and detection of ex-vivo breast cancer. *Photodiagnosis and Photodynamic Therapy* **2020**, *31*, 101922. https://doi.org/10.1016/j.pdpdt.2020.101922.
25. Alfano, R.R. Advances in ultrafast time resolved fluorescence physics for cancer detection in optical biopsy. *AIP Advances* **2012**, *2*, 011103. https://doi.org/10.1063/1.3697961.
26. Głowacz, K.; Skorupska, S.; Grabowska-Jadach, I.; Ciosek-Skibińska, P. Excitation–emission matrix fluorescence spectroscopy for cell viability testing in UV-treated cell culture. *RSC Advances* **2022**, *12*, 7652–7660. https://doi.org/10.1039/D1RA09021F.
27. Kalaivani, R.; Masilamani, V.; Sivaji, K.; Elangovan, M.; Selvaraj, V.; Balamurugan, S.; Al-Salhi, M. Fluorescence Spectra of Blood Components for Breast Cancer Diagnosis. *Photomedicine and Laser Surgery* **2008**, *26*, 251–256. https://doi.org/10.1089/pho.2007.2162.
28. Khosroshahi, M.E.; Rahmani, M. Detection and Evaluation of Normal and Malignant Cells Using Laser-Induced Fluorescence Spectroscopy. *Journal of Fluorescence* **2012**, *22*, 281–288. https://doi.org/10.1007/s10895-011-0958-4.
29. Karmakar, S.; Banik, N.L.; Patel, S.J.; Ray, S.K. 5-Aminolevulinic acid-based photodynamic therapy suppressed survival factors and activated proteases for apoptosis in human glioblastoma U87MG cells. *Neuroscience Letters* **2007**, *415*, 242–247. https://doi.org/10.1016/j.neulet.2007.01.071.
30. Aggarwal, V.; Tuli, H.; Varol, A.; Thakral, F.; Yerer, M.; Sak, K.; Varol, M.; Jain, A.; Khan, M.; Sethi, G. Role of Reactive Oxygen Species in Cancer Progression: Molecular Mechanisms and Recent Advancements. *Biomolecules* **2019**, *9*, 735. https://doi.org/10.3390/biom9110735.
31. Villalpando-Rodriguez, G.E.; Gibson, S.B. Reactive Oxygen Species (ROS) Regulates Different Types of Cell Death by Acting as a Rheostat. *Oxidative Medicine and Cellular Longevity* **2021**, *2021*, 1–17. https://doi.org/10.1155/2021/9912436.
32. Chance, B.; Salkovitz, I.; Kovach, A. Kinetics of mitochondrial flavoprotein and pyridine nucleotide in perfused heart. *American Journal of Physiology-Legacy Content* **1972**, *223*, 207–218. https://doi.org/10.1152/ajplegacy.1972.223.1.207.

 doi:10.20944/preprints202406.1312.v1

33. Shimizu, K.; Tamura, K.; Hara, S.; Inaji, M.; Tanaka, Y.; Kobayashi, D.; Sugawara, T.; Wakimoto, H.; Nariai, T.; Ishii, K.; et al. Correlation of Intraoperative 5-ALA-Induced Fluorescence Intensity and Preoperative 11C-Methionine PET Uptake in Glioma Surgery. *Cancers* **2022**, *14*, 1449. https://doi.org/10.3390/cancers14061449.
34. Molina, E.S.; Ewelt, C.; Warneke, N.; Schwake, M.; Müther, M.; Schipmann, S.; Stummer, W. Dual labeling with 5-aminolevulinic acid and fluorescein in high-grade glioma surgery with a prototype filter system built into a neurosurgical microscope: technical note. *Journal of Neurosurgery* **2020**, *132*, 1724–1730. https://doi.org/10.3171/2018.12.JNS182422.
35. (STRC), S.T.R.C. Stem Cell Technology Co and Cord Blood Bank/.
36. Netufo, O.; Connor, K.; Shiels, L.P.; Sweeney, K.J.; Wu, D.; O'Shea, D.F.; Byrne, A.T.; Miller, I.S. Refining Glioblastoma Surgery through the Use of Intra-Operative Fluorescence Imaging Agents. *Pharmaceuticals* **2022**, *15*, 550. https://doi.org/10.3390/ph15050550.
37. Ahrens, L.C.; Krabbenhøft, M.G.; Hansen, R.W.; Mikic, N.; Pedersen, C.B.; Poulsen, F.R.; Korshoej, A.R. Effect of 5-Aminolevulinic Acid and Sodium Fluorescein on the Extent of Resection in High-Grade Gliomas and Brain Metastasis. *Cancers* **2022**, *14*, 617. https://doi.org/10.3390/cancers14030617.
38. Hernot, S.; van Manen, L.; Debie, P.; Mieog, J.S.D.; Vahrmeijer, A.L. Latest developments in molecular tracers for fluorescence image-guided cancer surgery. *The Lancet Oncology* **2019**, *20*, e354–e367. https://doi.org/10.1016/S1470-2045(19)30317-1.
39. Joshi, B.P.; Wang, T.D. Targeted Optical Imaging Agents in Cancer: Focus on Clinical Applications. *Contrast Media & Molecular Imaging* **2018**, *2018*, 1–19. https://doi.org/10.1155/2018/2015237.
40. Nagaya, T.; Nakamura, Y.A.; Choyke, P.L.; Kobayashi, H. Fluorescence-Guided Surgery. *Frontiers in Oncology* **2017**, *7*. https://doi.org/10.3389/fonc.2017.00314.
41. Chung, C.W.; Chung.; Jeong, Y.I.; Kang, D.H. 5-aminolevulinic acid-incorporated nanoparticles of methoxy poly(ethylene glycol)-chitosan copolymer for photodynamic therapy. *International Journal of Nanomedicine* **2013**, p. 809. https://doi.org/10.2147/IJN.S39615.
42. Takahashi, J.; Nagasawa, S.; Doi, M.; Takahashi, M.; Narita, Y.; Yamamoto, J.; Ikemoto, M.J.; Iwahashi, H. In Vivo Study of the Efficacy and Safety of 5-Aminolevulinic Radiodynamic Therapy for Glioblastoma Fractionated Radiotherapy. *International Journal of Molecular Sciences* **2021**, *22*, 9762. https://doi.org/10.3390/ijms22189762.
43. Jia, P.; Dai, C.; Cao, P.; Sun, D.; Ouyang, R.; Miao, Y. The role of reactive oxygen species in tumor treatment. *RSC Advances* **2020**, *10*, 7740–7750. https://doi.org/10.1039/C9RA10539E.
44. Yang, H.; Villani, R.M.; Wang, H.; Simpson, M.J.; Roberts, M.S.; Tang, M.; Liang, X. The role of cellular reactive oxygen species in cancer chemotherapy. *Journal of Experimental & Clinical Cancer Research* **2018**, *37*, 266. https://doi.org/10.1186/s13046-018-0909-x.
45. Kohen, E.; Kohen, C.; Thorell, B. Rapid microfluorimetry of enzyme reactions in single living cells. *Biochimica et Biophysica Acta (BBA) - Bioenergetics* **1971**, *234*, 531–536. https://doi.org/10.1016/0005-2728(71)90223-4.
46. Lee, J.; Kim, B.; Park, B.; Won, Y.; Kim, S.Y.; Lee, S. Real-time cancer diagnosis of breast cancer using fluorescence lifetime endoscopy based on the pH. *Scientific Reports* **2021**, *11*, 16864. https://doi.org/10.1038/s41598-021-96531-0.
47. Katz-Brull, R.; Seger, D.; Rivenson-Segal, D.; Rushkin, E.; Degani, H. Metabolic markers of breast cancer: enhanced choline metabolism and reduced choline-ether-phospholipid synthesis. *Cancer research* **2002**, *62*, 1966–70.
48. Pu, Y.; Wang, W.; Yang, Y.; Alfano, R.R. Native fluorescence spectra of human cancerous and normal breast tissues analyzed with non-negative constraint methods. *Applied Optics* **2013**, *52*, 1293. https://doi.org/10.1364/AO.52.001293.
49. Heintzelman, D.L.; Lotan, R.; Richards-Kortum, R.R. Characterization of the autofluorescence of polymorphonuclear leukocytes, mononuclear leukocytes and cervical epithelial cancer cells for improved spectroscopic discrimination of inflammation from dysplasia. *Photochemistry and photobiology* **2000**, *71*, 327–32.
50. Nakamura, K.; Yoshikawa, N.; Yamaguchi, Y.; Kagota, S.; Shinozuka, K.; Kunitomo, M. Characterization of mouse melanoma cell lines by their mortal malignancy using an experimental metastatic model. *Life Sciences* **2002**, *70*, 791–798. https://doi.org/10.1016/S0024-3205(01)01454-0.

 doi:10.20944/preprints202406.1312.v1

51. Mousavikhamene, Z.; Sykora, D.J.; Mrksich, M.; Bagheri, N. Morphological features of single cells enable accurate automated classification of cancer from non-cancer cell lines. *Scientific Reports* **2021**, *11*, 24375. https://doi.org/10.1038/s41598-021-03813-8.
52. Malik, Z. Fundamentals of 5-aminolevulinic acid photodynamic therapy and diagnosis: An overview. *Translational Biophotonics* **2020**, *2*. https://doi.org/10.1002/tbio.201900022.
53. Razak, N.A.; Abu, N.; Ho, W.Y.; Zamberi, N.R.; Tan, S.W.; Alitheen, N.B.; Long, K.; Yeap, S.K. Cytotoxicity of eupatorin in MCF-7 and MDA-MB-231 human breast cancer cells via cell cycle arrest, anti-angiogenesis and induction of apoptosis. *Scientific Reports* **2019**, *9*, 1514. https://doi.org/10.1038/s41598-018-37796-w.
54. Kennedy, J.C.; Pottier, R.H. New trends in photobiology. *Journal of Photochemistry and Photobiology B: Biology* **1992**, *14*, 275–292. https://doi.org/10.1016/1011-1344(92)85108-7.
55. Howley, R.; Chandratre, S.; Chen, B. 5-Aminolevulinic Acid as a Theranostic Agent for Tumor Fluorescence Imaging and Photodynamic Therapy. *Bioengineering* **2023**, *10*, 496. https://doi.org/10.3390/bioengineering10040496.
56. Tsubone, T.M.; Martins, W.K.; Pavani, C.; Junqueira, H.C.; Itri, R.; Baptista, M.S. Enhanced efficiency of cell death by lysosome-specific photodamage. *Scientific Reports* **2017**, *7*, 6734. https://doi.org/10.1038/s41598-017-06788-7.
57. Kwiatkowski, S.; Knap, B.; Przystupski, D.; Saczko, J.; Kędzierska, E.; Knap-Czop, K.; Kotlińska, J.; Michel, O.; Kotowski, K.; Kulbacka, J. Photodynamic therapy–mechanisms, photosensitizers and combinations. *Biomedicine & Pharmacotherapy* **2018**, *106*, 1098–1107. https://doi.org/10.1016/j.biopha.2018.07.049.
58. Spring, B.Q.; Rizvi, I.; Xu, N.; Hasan, T. The role of photodynamic therapy in overcoming cancer drug resistance. *Photochemical & Photobiological Sciences* **2015**, *14*, 1476–1491. https://doi.org/10.1039/c4pp00495g.
59. van Straten, D.; Mashayekhi, V.; de Bruijn, H.; Oliveira, S.; Robinson, D. Oncologic Photodynamic Therapy: Basic Principles, Current Clinical Status and Future Directions. *Cancers* **2017**, *9*, 19. https://doi.org/10.3390/cancers9020019.
60. Galluzzi, L.; Vitale, I.; Aaronson, S.A.; Abrams, J.M.; Adam, D.; Agostinis, P.; Alnemri, E.S.; Altucci, L.; Amelio, I.; Andrews, D.W.; et al. Molecular mechanisms of cell death: recommendations of the Nomenclature Committee on Cell Death 2018. *Cell Death & Differentiation* **2018**, *25*, 486–541. https://doi.org/10.1038/s41418-017-0012-4.
61. Russo, C.A.M.; Voloch, C.M. Beads and Dice in a Genetic Drift Exercise. *Evolution: Education and Outreach* **2012**, *5*, 494–500. https://doi.org/10.1007/s12052-012-0438-6.
62. Klein, S.G.; Steckbauer, A.; Alsolami, S.M.; Arossa, S.; Parry, A.J.; Li, M.; Duarte, C.M. Toward Best Practices for Controlling Mammalian Cell Culture Environments. *Frontiers in Cell and Developmental Biology* **2022**, *10*. https://doi.org/10.3389/fcell.2022.788808.
63. Sayitoğlu, M. Clinical Interpretation of Genomic Variations. *Turkish Journal of Hematology* **2016**, *33*, 172–179. https://doi.org/10.4274/tjh.2016.0149.
64. Lin, X. Genomic Variation Prediction: A Summary From Different Views. *Frontiers in Cell and Developmental Biology* **2021**, *9*. https://doi.org/10.3389/fcell.2021.795883.
65. Gewers, F.L.; Ferreira, G.R.; Arruda, H.F.D.; Silva, F.N.; Comin, C.H.; Amancio, D.R.; Costa, L.D.F. Principal Component Analysis. *ACM Computing Surveys* **2022**, *54*, 1–34. https://doi.org/10.1145/3447755.